J. Fluid Mech. (2003), *vol.* 475, *pp.* 21–40.
DOI: 10.1017/S0022112002002811 Printed in the United Kingdom

Magnetohydrodynamic convection in a vertical slot with horizontal magnetic field

By ULRICH BURR[1]†, LEOPOLD BARLEON[2], PAUL JOCHMANN[3] AND ARKADY TSINOBER[4]

[1]Eidgenössische Technische Hochschule Zürich, Institut für Hydromechanik und Wasserwirtschaft, ETH Hönggerberg, CH-8093 Zürich, Switzerland

[2]Forschungszentrum Karlsruhe GmbH, Institut fuer Kern- und Energietechnik, Postfach 3640, D-76021 Karlsruhe, Germany

[3]Universität Karlsruhe, Institut für Thermische Strömungsmaschinen, Kaiserstrasse 12, D-76128 Karlsruhe, Germany

[4]Department of Fluid Mechanics and Heat Transfer, Faculty of Engineering, Tel Aviv University, Ramat Aviv, 69978 Tel Aviv, Israel

(Received 6 August 2001 and in revised form 28 August 2002)

This article presents an experimental study of magnetohydrodynamic convection in a tall vertical slot under the influence of a horizontal magnetic field. The test fluid is an eutectic sodium potassium $Na^{22}K^{78}$ alloy with a small Prandtl number of $Pr \approx 0.02$. The experimental setup covers Rayleigh numbers in the range $10^3 \lesssim Ra \lesssim 8 \times 10^4$ and Hartmann numbers $0 < M < 1600$. The effect of the magnetic field on the convective heat transport is determined not only by damping as expected from Joule dissipation but also, for magnetic fields not too strong, the convective heat transfer may be considerably enhanced compared to ordinary hydrodynamic (OHD) flow. Estimates of the isotropy properties of the flow by a four-element temperature probe demonstrate that the increase in convective heat transport accompanies the formation of strong local anisotropy of the turbulent eddies in the sense of an alignment of the main direction of vorticity with the magnetic field. The reduced three-dimensional nonlinearities in non-isotropic flow favour the formation of large-scale vortex structures compared to OHD flow, which are more effective for convective heat transport. Along with the formation of quasi-two-dimensional vortex structures, temperature fluctuations may be considerably enhanced in a magnetic field that is not too strong. However, above Hartmann numbers $M \gtrsim 400$ the formerly strongly time-dependent flow suddenly becomes stationary with an extended region of high convective heat transport at stationary flow. Finally, for very high Hartmann numbers the convective motion is strongly suppressed and the heat transport is reduced to a state close to pure heat conduction.

1. Introduction

Buoyancy-driven flow in a tall vertical enclosure is one of the fundamental problems of convective heat transport with simple well-defined boundary conditions. Moreover, even in the case of liquid metal, it is of significant importance in many engineering applications such as liquid metal cooling in power engineering, metallurgical melting

† Present address: Voith Turbo GmbH & Co. KG, Alexanderstrasse 2, 89522 Heidenheim, Germany.

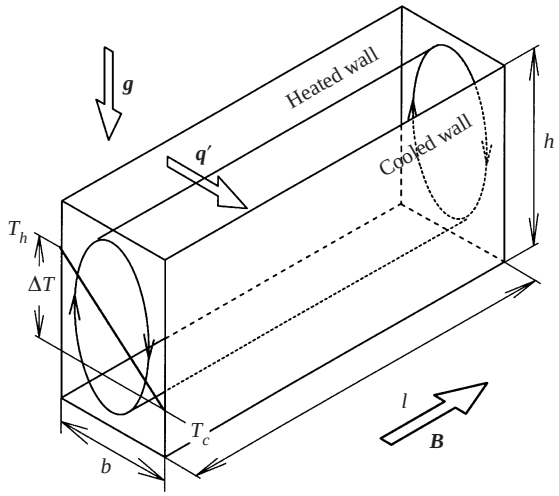

FIGURE 1. Geometry of the flow problem investigated.

and solidification processes, e.g. in crystal growth processes. Due to the high electrical conductivity of liquid metals the flow may be influenced by external magnetic fields. For instance, magnetohydrodynamic (MHD) flow control can be designed to optimize production processes. In figure 1 the flow problem under consideration is sketched. Liquid metal is confined in a rectangular enclosure of width b, length l and height h and non-slip boundary conditions hold at all walls. The left-hand vertical wall is heated and the opposite one is cooled so that a temperature difference ΔT and an associated heat flux $\boldsymbol{q}$ is maintained across the gap, perpendicular to the acceleration due to gravity $\boldsymbol{g}$. All the other walls are thermally insulated. A homogeneous magnetic field $\boldsymbol{B}$ may be imposed in the horizontal direction perpendicular to the applied heat flux, i.e. the transversal direction.

The geometry of the cavity is characterized by the two aspect ratios $A_1 = h/b$ and $A_2 = l/b$. The buoyant flow of a Newtonian fluid under ordinary hydrodynamic (OHD) conditions is governed by two independent dimensionless groups. The Rayleigh number

$$Ra = \frac{\beta g \Delta T b^3}{\nu \kappa}, \tag{1}$$

represents the driving force of convection, where β is the thermal expansion coefficient, g the magnitude of the acceleration due to gravity, ν the kinematic viscosity and $\kappa = \lambda/\rho c_p$ the thermal diffusivity with the thermal conductivity λ, the density ρ and the specific heat capacity c_p. The Prandtl number

$$Pr = \frac{\nu}{\kappa} \tag{2}$$

is the ratio of the thermal and the viscous diffusion time and characterizes diffusive properties of the fluid. The effectivity of the convective heat transport is characterized by the dimensionless Nusselt number

$$Nu = \frac{q}{q_0} \tag{3}$$

defined as the ratio of the total heat flux q to the conductive heat flux $q_0 = -\lambda \Delta T/b$.

If a magnetic field $\boldsymbol{B}$ is imposed, electric currents $\boldsymbol{j}$ are induced by the convective

motions and the flow becomes governed by two additional dimensionless parameters: the magnetic Reynolds number

$$Rm = \mu\sigma v_0 b \tag{4}$$

and the Chandrasekhar number

$$Q = M^2 = \frac{B^2 b^2 \sigma}{\rho \nu}, \tag{5}$$

which is the square of the Hartmann number M commonly used in MHD duct flows and in what follows. In these definitions, μ is the magnetic permeability, σ the electrical conductivity, v_0 some characteristic velocity of the fluid produced by the buoyant forces and B the magnitude of magnetic induction. The magnetic Reynolds number gives the ratio of the magnetic field induced by the fluid motion to the applied external magnetic field. The Chandrasekhar number denotes the ratio of the Lorenz forces $\boldsymbol{F}_L = \boldsymbol{j} \times \boldsymbol{B}$, that are produced by the interaction of the current density $\boldsymbol{j}$ with the applied magnetic field $\boldsymbol{B}$, to the viscous forces. Well-known estimates show that the induced magnetic field may be neglected in the flow configurations discussed here and either Q or M is the only relevant additional parameter related to the applied magnetic field.

In MHD flows the electrical properties of walls have a significant influence. They are combined in a dimensionless form as the wall conductance ratio

$$c = \frac{\sigma_W s}{\sigma b}, \tag{6}$$

where σ_W is the electrical conductivity of the wall material and s is the thickness of the wall considered (see e.g. Walker 1981).

Under ordinary hydrodynamic (OHD) conditions the different flow regions in the parameter space of Rayleigh number and ordinary fluid Prandtl number $Pr \gtrsim 1$ are well established in the literature. For a review see e.g. Gebhart *et al.* (1988). For very small Rayleigh numbers a stationary unicellular convective motion is established. At small enough convective velocities the fluid temperature remains almost uniform along the height and heat is mainly transported by heat conduction. As the Rayleigh number is increased convective motions become stronger and the contribution of convective heat transport is increased. A vertical temperature gradient develops in the core and a boundary layer type flow develops at the vertical walls. This *primary flow* region becomes unstable to either stable multicellular convective patterns or travelling waves. From the analysis of Vest & Arpaci (1969) and Bergholz (1977) it is established that, for Prandtl numbers $Pr < 12.7$, stable multicellular patterns of 'cat's eye' type, called *secondary flows* occur for $Gr > 7880$, where $Gr = Ra/Pr$ is the Grashof number. Other stationary flows (*tertiary flows*) characterized by regions of reversed circulation between the secondary cells (see Elder 1965) may follow this transition but, finally, the flow becomes time-dependent and then turbulent except in the thin boundary layers at the top and bottom walls.

Along with the flow patterns, the Nusselt number depends on all the parameters including both aspect ratios. Scaling with the Grashof number may sometimes be appropriate, but heat transfer correlations derived for ordinary fluids with $Pr \gtrsim 1$ are generally not valid for liquid metals with Prandtl numbers $Pr \ll 1$. Nevertheless, only a few studies of the OHD flow are focused on low Prandtl number fluids. Papailiou & Lykoudis (1974) investigated turbulent boundary layer flow in mercury ($Pr = 0.026$) developing along vertical walls. Gill (1974) treated theoretically the occurrence of oscillating flow in OHD flow and compared his results with experimental data mainly

obtained by Hurle, Jackeman & Johnson (1974). Depending on the aspect ratios, time-dependent flow occurs for Rayleigh numbers of $O(10^3)$. Hurle *et al.* (1974) also reported that a transverse magnetic field may quench the oscillations and steady convective motion may be obtained at higher Rayleigh numbers than for OHD flow. Moreover, there is also a significant influence of magnetic field on the convective heat transport. Emery (1963) showed that in mercury flow the convective heat flux is significantly reduced by a magnetic field imposed in the horizontal direction parallel to the heat flux. Similar findings were obtained by Papailiou & Lykoudis (1968) for a transversal magnetic field. Ozoe & Okada (1989) showed by numerical simulation and later in an experiment (Okada & Ozoe 1992) that externally applied magnetic fields in all three directions damp the convective motions in a cubic enclosure. Diminishing of the convective heat transport was observed to be minimal if the magnetic field was applied in the transversal direction whereas the highest damping was obtained for a horizontal magnetic field paralell to the direction of the applied heat flux. Such a damping effect is easily explained by Joule dissipation arising from the presence of a current density in the fluid. However, the magnetic field does not only suppress the flow. Experiments of Fumizawa (1980) have shown that a transverse magnetic field may under certain conditions also enhance the convective heat transport compared to the OHD flow. Similar findings have been reported recently by Burr & Müller (2002) in Rayleigh–Bénard convection with an imposed horizontal magnetic field. The effect can be explained by an ordering effect of the magnetic field on the three-dimensional convective vortex motion caused by the non-isotropic character of the Lorenz forces (see also Sommeria & Moreau 1982 and Davidson 1995). Namely, vorticity lines tend to become aligned with the magnetic field and thereby Joule dissipation is considerably reduced. Hence, the flow properties like the convective heat flux are governed by co-existing mechanisms. On the one hand the convective velocities and, consequently, the convective heat transfer is generally reduced by Joule dissipation. On the other hand this damping effect may be compensated due to suppression of three-dimensional flow structures and favouring of two-dimensionality. Two-dimensional large-scale coherent vortex structures are very effective in convective transport. If the formation of two-dimensional flow structures over-rides the damping effect of Joule dissipation an increase of the convective heat transfer may be expected. Thus we also address the occurrence of a quasi-two-dimensional flow at very high Hartmann numbers (see e.g. Sommeria & Moreau 1982 and Burr & Müller 2002) where the flow is two-dimensional in a core region but not in thin boundary layers at walls perpendicular to the magnetic field (Hartmann walls).

Both the drastic changes of the flow structure and the control of the heat transfer are very attractive features and there has recently been a growing interest motivated by industrial applications mentioned above.

This paper aims to provide new information on the integral heat transfer and flow characteristics in a broad range of accessible Rayleigh and Hartmann numbers and, moreover, to link these phenomena to local isotropy properties of the flow in order to contribute to the understanding of general phenomena in MHD convection. It is organized as follows: In the next section a brief description of the experimental setup is given. In § 3 experimental results concerning the integral flow properties such as heat transfer rates and the transition from stationary to time-dependent flow evaluated from a systematic test matrix are presented. The specific temporal and spatial structure of the flow is discussed in a separate subsection. In § 4 the results are summarized and some conclusions are drawn.

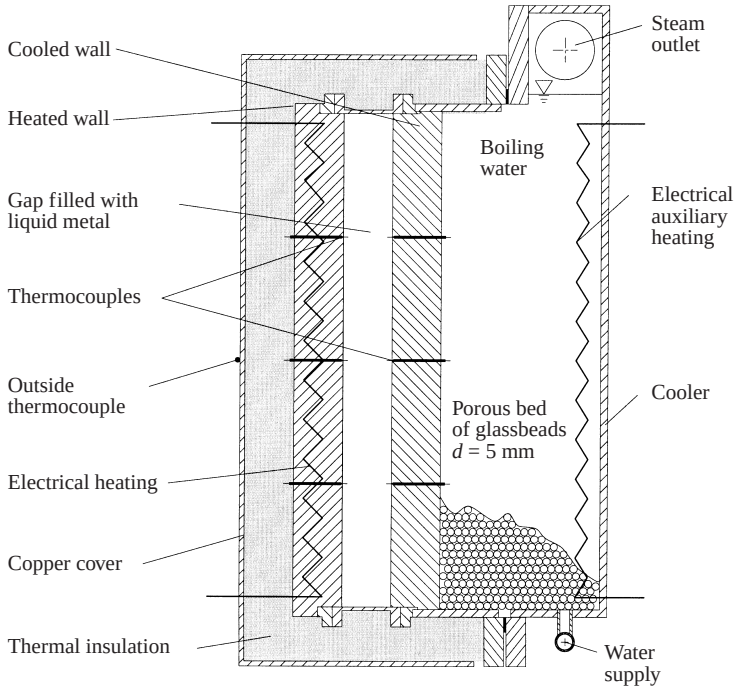

FIGURE 2. Vertical cross-section (plane perpendicular to the magnetic field) of the test section showing some technical details.

2. Experimental setup and performance

The test section provides a vertical gap of width $b = 20\,\text{mm}$, height $h = 200\,\text{mm}$ and length $l = 400\,\text{mm}$ (see figure 1). Thus the two aspect ratios defined in § 1 are large, i.e. $A_1 = 10$ and $A_2 = 20$. A vertical cross-section, showing some technical details, is given in figure 2. The gap is filled with a test fluid which is an eutectic sodium potassium alloy $Na^{22}K^{78}$, with 22% weight sodium and 78% weight potassium. The temperature-dependent thermophysical properties are calculated for the mean temperature of the fluid T_m based on fitting curves derived from data taken from O'Donnel, Papanicolaou & Reed (1989), Lyon (1952) and Foust (1972). The Prandtl number varies in the range $0.017 < Pr < 0.021$ because of the temperature dependence of the physical properties. The heated and the cooled vertical walls are 20 mm thick copper plates. Due to the high thermal conductivity of copper compared to NaK they provide to a best approximation isothermal boundary conditions. All other walls facing the fluid are 1.5 mm thick stainless steel sheets and are thermally insulated from the environment. As the thermal conductivity of stainless steel is significantly smaller than that of the test fluid their influence on the temperature distribution of the fluid may be neglected. From definition (6) the wall conductance ratios for the copper and the stainless steel walls are calculated as $c_{Cu} \approx 4.5$ and $c_{ss} \approx 0.08$. The hot wall is heated electrically with a maximum power of $P \approx 7200\,\text{W}$ giving a maximum heat flux of $q \approx 8.8 \times 10^4\,\text{W m}^{-2}$ and resulting in Rayleigh numbers up to $Ra \lesssim 10^5$. In order to calculate the heat flux q from the measured power of the electrical heating, three different sources of heat losses have been taken into account. First, there is heat loss by conduction through the thermal insulation, which was determined by separate tests for situations with no heat flux across the gap; it is considered in

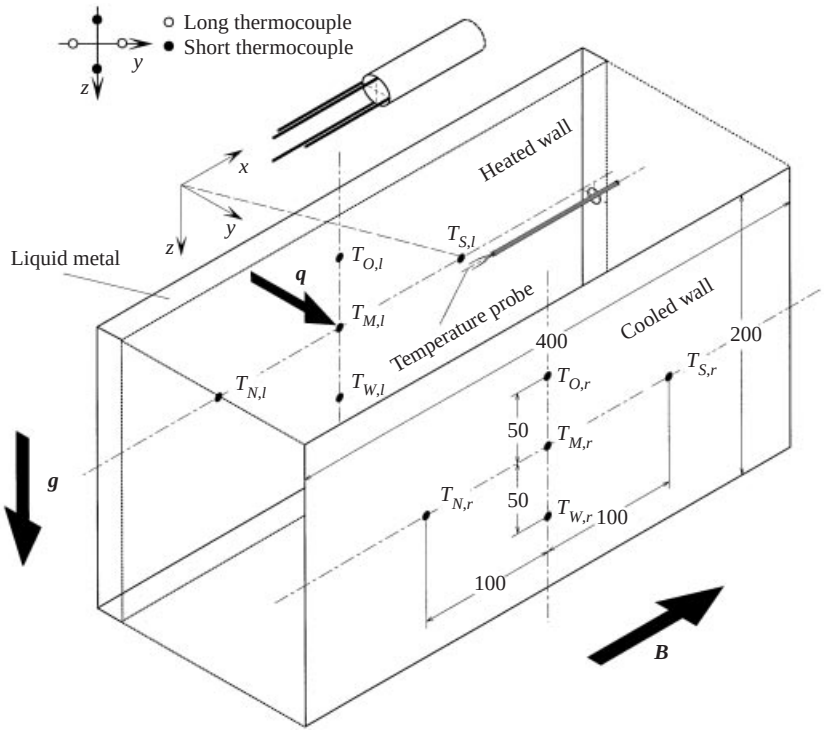

FIGURE 3. Instrumentations of the heat transfer test facility and schematic of the sensing tip of the four-element temperature probe placed in the centre of the gap. All lengths measures are given in mm.

the evaluations of q as a functional of the temperature difference between the hot wall and the temperature of the near environment. The latter was measured by a separate thermocouple on the copper cover of the facility. Second, there is also heat conduction through the sidewalls, which can easily be calculated from Fourier's law using the temperature difference between the copper plates. Third, there are Ohm's losses in the wiring and cold ends of the heater rods which is proportional to the applied electrical power.

The heat transferred through the liquid layer is removed from the cooled wall by boiling water in a porous bed consisting of glassbeads of 5 mm in diameter. The water is kept at boiling temperature by an auxiliary heater and thus the heat is removed from the wall by the boiling process only and a uniform temperature at the wall is obtained. The steam is removed from the top and condensed in an external water-cooled atmospheric condenser. The condensed water is preheated and fed back by pipes at the lower side of the cooler.

The test section is placed into the bore of a superconducting magnet which can generate a horizontal magnetic field of up to 3.5 T and which is constant to a spatial accuracy better than $\pm 4\%$. In this investigation tests were conducted only in the range of Hartmann numbers $0 < M < 1600$.

In figure 3 the instrumentations of the test section are sketched and their precise positions are given. Five Cu–CuNi thermocouples are embedded in each copper plate and are positioned at a distance 1 mm from the fluid–wall interface. The temperature difference across the layer $\Delta T = T_h - T_c$ and the mean temperature of the fluid

$T_m = (T_h + T_c)/2$ are evaluated from the five temperatures $T_{i,j}$ in each wall as a spatial and temporal average. Here, T_h and T_c denote the mean temperatures of the heated and the cooled wall, respectively (see figure 1). Physical properties as well as characteristic numbers are always evaluated from temporal mean values and therefore the averaging is not mentioned further. Temporal mean values are denoted by an overbar whereas fluctuating parts are denoted by a prime. The local time-dependent properties in the centre of the liquid metal layer, between the thermocouples $T_{S,l}$ and $T_{S,r}$, are measured by using a four-element temperature probe which can sense the fluctuating parts of temperature T'_P and the local temperature gradient $\nabla T'_P = (\partial_x T'_P, \partial_y T'_P, \partial_z T'_P)$. The latter measurement is performed by a non-coplanar arrangement of four shielded Ni–CrNi thermocouples each of 0.25 mm diameter which protrude from an insulating ceramics tube with a diameter of 2 mm. The geometry of the probe is sketched in the upper part of figure 3. The lateral distance between the two long and the two short thermocouples is 2 mm whereas the long thermocouples are 1.4 mm longer than the shorter ones. For a more detailed description of the probe geometry see Burr & Müller (2001). Here, the four thermocouples have been connected to the data acquisition system in such a way that one element measures the temperature of the fluid with reference to an ice point whereas the three others are connected in reference to the first one to sense directly the temperature difference. The gradient vector thus obtained in a coordinate system defined by the thermocouple positions may be transferred into the coordinate system of the test section by vector transformation. This arrangement allows a high amplification of the gradient signals and produces much less noise than calculating the temperature gradients from independently measured temperature values.

The definition of isotropy coefficients

$$A_{ij} = \frac{\overline{(\partial_i T_P)'^2}}{\overline{(\partial_j T_P)'^2}}, \quad i, j = x, y, z, \tag{7}$$

allows an objective estimate of the local isotropy properties of the time-dependent motions, where $\overline{(\partial_i T_P)'^2}$ is the variance of the temperature gradient in the i-direction. If all coefficients approach unity, the flow may be called locally isotropic. If i refers to the x-direction the two transversal coefficients A_{xy} and A_{xz} indicate non-isotropy in the direction of the magnetic field in terms of weaker fluctuations in the direction of the magnetic field. It is reasonable to evaluate the trend towards a two-dimensional velocity field from decreasing values of the transversal isotropy coefficients. However, the flow still may be isotropic in the vertical plane perpendicular to the magnetic field which is indicated by the vertical isotropy coefficient $A_{yz} \approx 1$.

3. Experimental results

3.1. *Integral flow properties*

As a first step, the influence of the magnetic field at six Hartmann numbers, including OHD flow, on the integral flow properties is investigated in a test series with increasing heating power at fixed steps in the range $200 < P < 7200$ W. The Hartmann numbers M and the approximate magnitudes of the magnetic field B are summarized in table 1.

If not mentioned otherwise, the experimental results are presented in dimensionless form by using the width of the gap b, the temperature difference across the layer ΔT, the thermal diffusion time $t_0 = b^2/\kappa$ and its inverse $f_0 = 1/t_0$ as scales for length, temperature, time and frequency.

M	0	100	200	400	800	1600
$B\,[T]$	0	0.07	0.15	0.29	0.58	1.16
Ra_t	–	–	–	1×10^4	4×10^4	8×10^4

TABLE 1. Hartmann numbers M, approximate magnitude of the applied magnetic field B and critical Rayleigh number Ra_t for the onset of time-dependent flow.

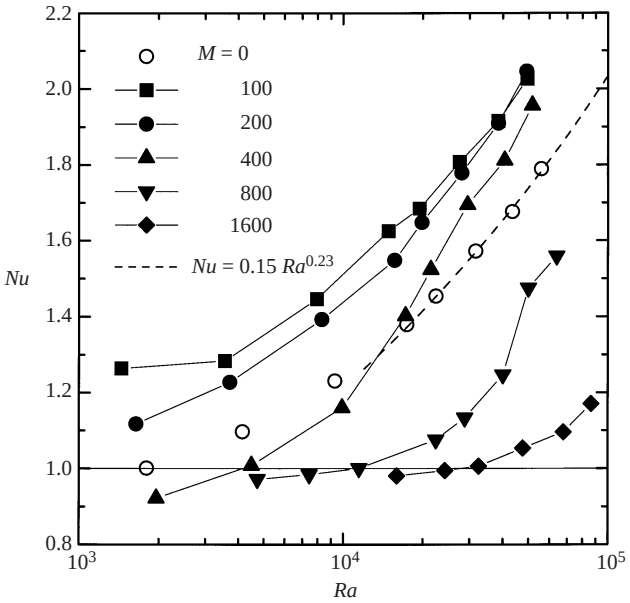

FIGURE 4. Nusselt numbers Nu versus Rayleigh numbers Ra for OHD flow (open circles) and MHD flows (solid symbols).

The Nusselt numbers obtained are plotted versus the Rayleigh numbers in figure 4. Consider first the case of OHD flow ($M = 0$) denoted by the open circles. For the lowest heating power $P = 200\,\mathrm{W}$ a temperature difference across the layer of $\Delta T = 1.35\,\mathrm{K}$ corresponding to a Rayleigh number of $Ra = 1789.6$ is obtained. Based on the results by Vest & Arpaci (1969) and Bergholz (1977) we may assume that a multicellular secondary flow exists. However the convective velocities are low and the heat transfer is close to the state of pure heat conduction. Starting from this point, the Nusselt number increases continuously with increasing Rayleigh number. For high Rayleigh numbers a scaling law $Nu = 0.15 \times Ra^{0.23\pm0.02}$ is valid in the range $10^4 < Ra < 10^5$, which is plotted as a dashed line in figure 4. When a magnetic field is applied one could expect a general decrease of the convective heat transport because of the damping effect of Joule dissipation. However, this is not observed in general. All measured Nusselt numbers for $M = 100$ and $M = 200$ are higher than for the OHD flow. For $M = 400$ the Nusselt numbers at low Rayleigh number are lower than those for OHD flow but are greater for $Ra \gtrsim 10^4$. Then, for the high Hartmann numbers $M = 800$ and $M = 1600$ the convective heat transfer is significantly reduced compared to OHD flow in the whole range of Rayleigh numbers investigated here. This demonstrates the existence of the two opposing effects of the magnetic field

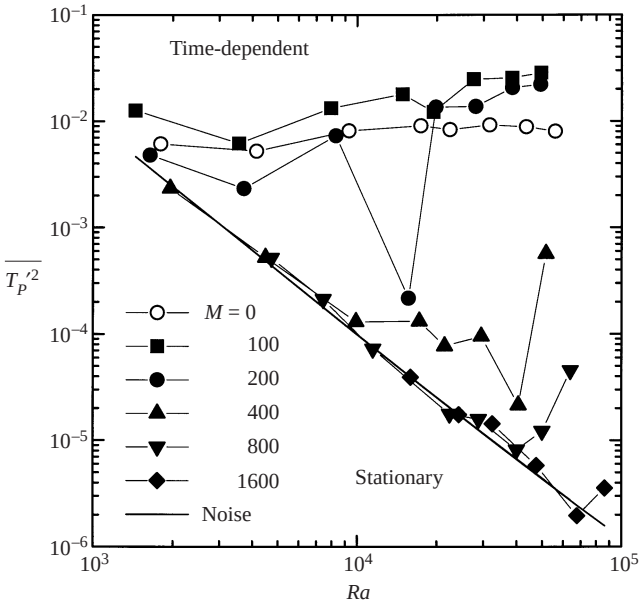

FIGURE 5. Variances of temperature $\overline{T_P'^2}$ recorded by the probe for OHD flow (open circles) and MHD flows at different Hartmann numbers M (solid symbols).

on the convective heat transport, namely the formation of strongly non-isotropic structure on the one hand, and Joule dissipation on the other.

It should be mentioned that the Nusselt numbers $Nu < 1$ plotted in figure 4 are in principle non-physical because they would indicate less heat transport than in the case of pure heat conduction. Since the applied heat flux q and the temperature difference ΔT used in the calculation of Nu from equation (3) are determined with much higher accuracy than would explain such large errors the deviation from $Nu = 1$ most probably results from errors in the values for the temperature-dependent thermal conductivity λ of the NaK test fluid used for the evaluations.

The next question addressed is whether the flow is stationary or time-dependent and how strong are the fluctuations in the time-dependent regime. This information is obtained from the variance of the temperature signal $\overline{T_P'^2}$ of the probe. It is plotted in figure 5 as a function of Rayleigh number. The solid line scaling as Ra^{-2} is the level of noise, which is determined separately from thermally neutral instrumentation tests. For states below this line the flow is considered to be stationary whereas time-dependent flow is assumed for values above. For OHD flow as well as for MHD flow at Hartmann numbers $M = 100$ and $M = 200$ all variances are significantly higher than the noise level and the flow is therefore considered to be time-dependent even for the lowest Rayleigh numbers. At higher Hartmann numbers $M = 400$, $M = 800$ and $M = 1600$ the values of $\overline{T_P'^2}$ emerge from the noise level at some critical Rayleigh number and a critical Rayleigh number for the onset of time-dependent flow Ra_t can be associated with the location of branching from the measurements. The obtained values are compiled in table 1. The variances, i.e. the temperature fluctuations for the smaller magnetic fields $M \leqslant 200$, significantly exceed the values obtained for OHD flow especially at Rayleigh numbers $Ra > 2 \times 10^4$ in spite of the presence of Joule dissipation. Thus, depending on its strength, the magnetic field is able to either enhance fluctuations of the velocity and the temperature fields or on the

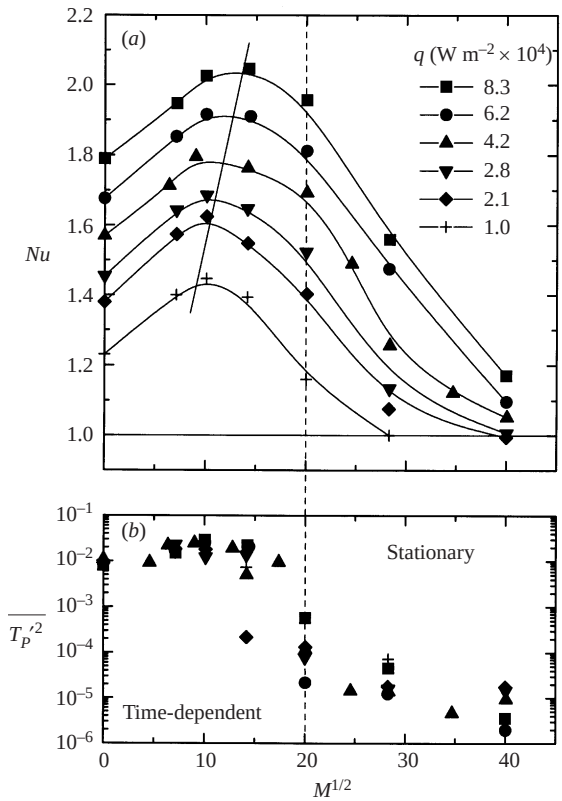

FIGURE 6. (*a*) Nusselt number Nu versus square root of the Hartmann number $M^{1/2}$ for different fixed heat fluxes q. (*b*) Corresponding variances of temperature fluctuations $\overline{T_P'^2}$ recorded by the probe.

contrary to suppress time-dependent flow resulting in a stationary flow. The large scatter of data, which becomes more pronounced at higher Hartmann numbers, most probably results from several bifurcations of the convective flow in the transition regime from stationary to strongly time-dependent flow. A systematic investigation of this phenomenon was not performed in these experiments.

Many heat transfer problems are defined with constant heat fluxes at the boundaries ($q = \text{const}$). This situation can be rendered by a constant product of Rayleigh and Nusselt numbers, i.e. $Ra \times Nu = \text{const}$. In figure 6(*a*) the Nusselt numbers are plotted versus the square root of the Hartmann number $M^{1/2}$ for different values of the applied heat flux. The Nusselt numbers increase from the values of OHD flow to a maximum value which is obtained in the range $10 < M^{1/2} < 15$ with a tendency of higher Hartmann numbers at larger heat fluxes. From this maximum value the Nusselt numbers decrease monotonically to values close to $Nu = 1$ for increasing Hartmann numbers. In table 2 the heat flux and the corresponding $Ra \times Nu$ values are listed. They allow calculation of the corresponding Rayleigh numbers from the Nusselt numbers given in figure 6(*a*). It is obvious from table 2 that the temperature difference or Rayleigh number decreases if the Nusselt number is increased at some fixed heat flux.

In figure 6(*b*) the variances of temperature fluctuations $\overline{T_P'^2}$, measured by the probe, are plotted. For Hartmann numbers $M \lesssim 400$ the variance values indicate strong

q [W m^{-2} $\times$ 10^4]	1.0	2.1	2.8	4.2	6.2	8.3
$Ra \times Nu$ [10^4]	1.15	2.41	3.27	5.00	7.36	10.02

TABLE 2. Heat fuxes q and corresponding values of $RaNu$.

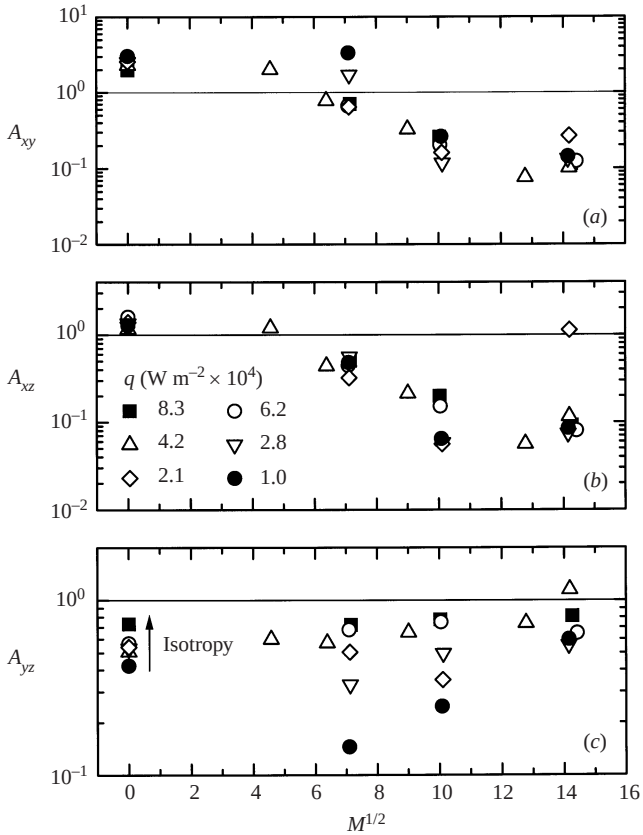

FIGURE 7. Isotropy coefficients A_{ij} as a function of square root of Hartmann number $M^{1/2}$ at different constant heat fluxes q: (a,b) the transversal coefficients A_{xy} and A_{xz}; (c) the vertical coefficient A_{yz}.

time-dependent motion. For higher Hartmann numbers the variances drop abruptly by several orders of magnitude indicating a stationary flow for Hartmann numbers $M \gtrsim 400$. Considering the Nusselt numbers and variances in figures 6(a) and 6(b) we find on the right-hand side of the dashed line significant convective heat transfer in an extended region of stationary flow.

In the time-dependent region for $M < 400$ we used the capability of the probe to measure fluctuations of the temperature gradient also and calculate the isotropy coefficients defined from equation (7). In figures 7(a) and 7(b) the two transversal coefficients A_{xy} and A_{xz} are plotted versus the square root of the Hartmann number $M^{1/2}$ at constant heat flux q. Figure 7(c) shows the vertical coefficient A_{yz} obtained in the plane perpendicular to the magnetic field. First we consider the case $M = 0$ of OHD flow. Both transversal coefficients A_{xy} and A_{xz} are larger than one and therefore indicate stronger fluctuations in the x-direction. The vertical coefficient A_{yz} indicates

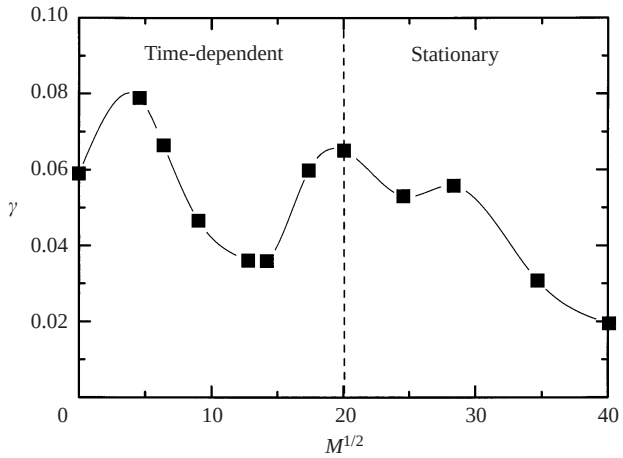

FIGURE 8. Relative vertical temperature gradient $\gamma = (T_{O,l} - T_{W,l})/(5\Delta T)$ as a function of the square root of the Hartmann number $M^{1/2}$ for a fixed heat flux of $q = 4.2 \times 10^4\,\mathrm{W\,m^{-2}}$.

much less intensive fluctuations in the direction of the heat flux compared to the vertical direction. However, as the heat flux increases the flow proceeds to a state of higher local isotropy indicated by the tendency of A_{yz} to approach the value 1. Next we consider the case of MHD flow. Above $M^{1/2} \gtrsim 6$ both transversal isotropy coefficients start to decrease strongly and at $M^{1/2} \gtrsim 10$ level off to plateau values more than an order of magnitude lower than in the case of no magnetic field. This indicates the formation of significant local non-isotropy implying weaker fluctuations in the direction of the magnetic field and time-dependent convective vortices whose axes are predominantly aligned with the direction of the magnetic field. This transition corresponds to the region of increasing Nusselt numbers seen in figure 6(*a*) and we suggest that this mechanism is responsible for the enhanced convective heat transport. Above $M^{1/2} \gtrsim 10$, non-isotropy is maintained, but the Joule dissipation becomes more and more dominant and leads to a decrease of the Nusselt numbers.

The vertical isotropy coefficient A_{yz} plotted in figure 7(*c*) increases considerably with M. Thus we can conclude that at strong enough magnetic fields the flow becomes more isotropic in the plane perpendicular to its direction. For all M there is a strong tendency towards higher isotropy in the plane perpendicular to the magnetic field as the heat flux is increased.

The next question is how the magnetic field changes the global flow structure. From two of the thermocouples embedded in the heated wall, $T_{O,l}$ and $T_{W,l}$ (see figure 3) we calculate the parameter $\gamma = (T_{O,l} - T_{W,l})/(5\Delta T)$ as an estimate of the relative vertical temperature gradient. The result for a fixed heat flux of $q = 4.2 \times 10^4\,\mathrm{W\,m^{-2}}$ is plotted in figure 8 versus the square root of the Hartmann number $M^{1/2}$. The Rayleigh numbers in this experiment are in the range $3.0 \times 10^4 < Ra < 5.0 \times 10^4$. Under OHD conditions we find a significant vertical temperature gradient, indicating that there is a considerable heat transport by a large-scale convection extending from top to bottom of the slot. Nevertheless, there may be smaller-scale flow structures. The contribution of the large-scale transport is more significant for the smallest Hartmann number $M^{1/2} = 4.5$ but as M is increased up to $M^{1/2} \approx 15$ the vertical temperature gradient is continuously decreased. From this we infer that the large-scale recirculation becomes suppressed and the multicellular motion becomes more

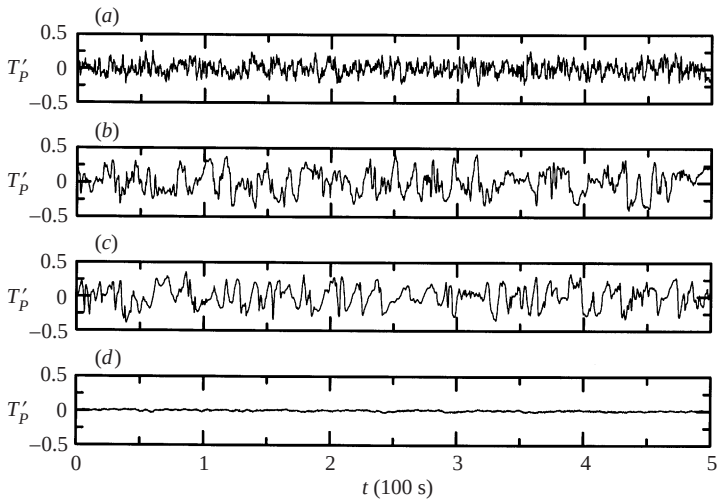

FIGURE 9. Time series of temperature fluctuations obtained from the probe T'_P at $Ra = 4.0 \times 10^4$. (*a*) OHD flow at $M = 0$; and MHD flow at Hartmann numbers (*b*) $M = 100$, (*c*) $M = 200$ and (*d*) $M = 400$.

important for the heat transport at higher magnetic fields. In the transition region from time-dependent to stationary flow, $15 < M^{1/2} < 20$, γ increases again suggesting a collapse of the multicellular pattern due to the reduced convective velocities and the formation of a unicellular convective motion as is known in OHD flow for small Rayleigh numbers in the primary flow region. In the stationary regime γ decreases monotonically with M, indicating that heat transport is increasingly dominated by conductive transport.

3.2. *Temporal characteristics*

Next we analyse the structure of the time-dependent signals obtained by the probe. Measurements were performed at a constant Rayleigh number $Ra = 4.0 \times 10^4$ and for Hartmann numbers $M = 0$, $M = 100$, $M = 200$ and $M = 400$. In figure 9(*a–d*) the time series are plotted. For OHD flow ($M = 0$) there is a typical turbulent signal characterized by random fluctuations of different time scales. When a magnetic field corresponding to $M = 100$ and $M = 200$ was applied the amplitudes of fluctuations were increased considerably. Moreover, the signals show fluctuations of longer time scales. Finally at $M = 400$ there is stationary flow. These findings are reflected well in the phase-averaged power spectra S of the temperature signals plotted in figure 10(*a*). Under MHD conditions the contribution of frequencies above $f \approx 4$ to the fluctuating intensity is significantly reduced whereas contributions below $f \approx 4$ are significantly enhanced compared to OHD convection. This power shift from higher to lower frequencies within the overall spectrum can be associated with the formation of motions with larger spatial scale under the influence of the magnetic field, provided that the Taylor hypothesis is valid. It is caused by the reduction of three-dimensional nonlinearities in the locally non-isotropic flow caused by the magnetic field. The spectra of OHD flow as well as those of MHD flow decay in the high-frequency range as f^{-4}. Similar scaling has been observed in liquid metal Rayleigh–Bénard convection under OHD conditions by Horanyi, Krebs & Müller (1999) and by Kishida & Takeda (1994) in the case of a strong applied magnetic field. The insets in figure 10(*a*), i.e. figures 10(*b*) and 10(*c*), show the corresponding variances $\overline{T'^2_P}$ and

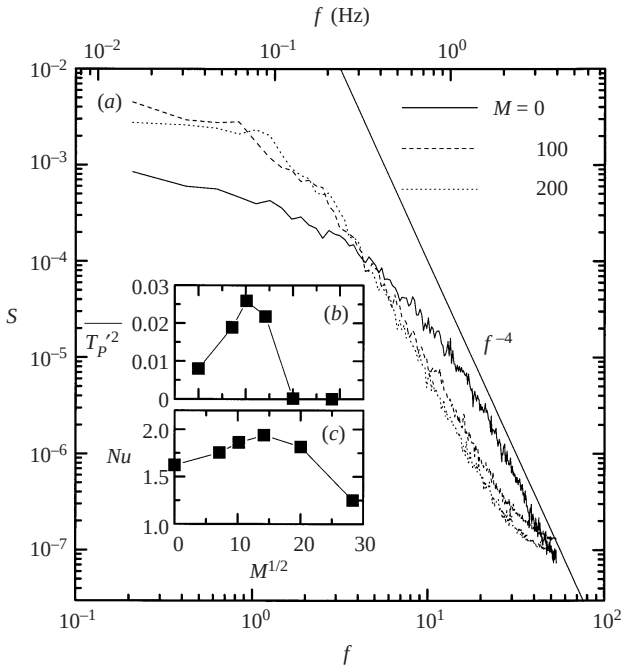

FIGURE 10. (*a*) Phase-averaged power spectra S of temperature fluctuations T'_P recorded by the probe at $Ra = 4.0 \times 10^4$ for OHD flow ($M = 0$) and for Hartmann numbers $M = 100$ and $M = 200$. (*b*) Variance $\overline{T'^2}$ and (*c*) Nusselt number Nu as a function of the square root of Hartmann number $M^{1/2}$.

the Nusselt numbers Nu. It is obvious that the change in the convective structure accompanies an enhancement of the fluctuating intensity as well as the convective heat transfer.

An intuitive picture of the isotropy properties of the velocity field is obtained from the scatter plots of the two-dimensional temperature gradient vectors $\nabla_{ij} T'_P = (\partial_i T'_P, \partial_j T'_P)$ which are plotted in figure 11(*a–l*) for the same data as shown in figure 9(*a–d*). The first two columns show the scatter plots in the transversal x-direction, aligned with the magnetic field, $\nabla_{xy} T'_P$ and $\nabla_{xz} T'_P$, whereas the third column shows the scatter in the vertical plane perpendicular to the magnetic field $\nabla_{yz} T'_P$. The first row corresponds to $M = 0$ and the magnetic field is increased from top to bottom.

For OHD flow both scatter plots containing the transversal direction, i.e. figure 11(*a*, *b*), are characterized by an almost axisymmetric distribution of the gradient vectors which can be associated with a high degree of isotropy in both planes. Under the influence of the magnetic field fluctuations in the transversal direction are considerably reduced. This is seen from figures 11(*d*) and 11(*e*) for $M = 100$ and figures 11(*g*) and 11(*h*) for $M = 200$ from the narrow band of the distributions of the gradient vectors in the x-direction. Simultaneously, the fluctuations of the temperature gradients in directions not aligned with the magnetic field are enhanced and the distributions become skewed in the negative y-direction and the positive z-direction, respectively. In the plane perpendicular to the magnetic field the fluctuations of the temperature gradients are not even isotropic for OHD flow (figure 11*c*). The distributions become skewed with respect to the negative y-direction and the positive z-direction when a magnetic field is applied (figures 11*f* and 11*i*). But even here a tendency to higher isotropy in this plane is observed, consistent with the findings in

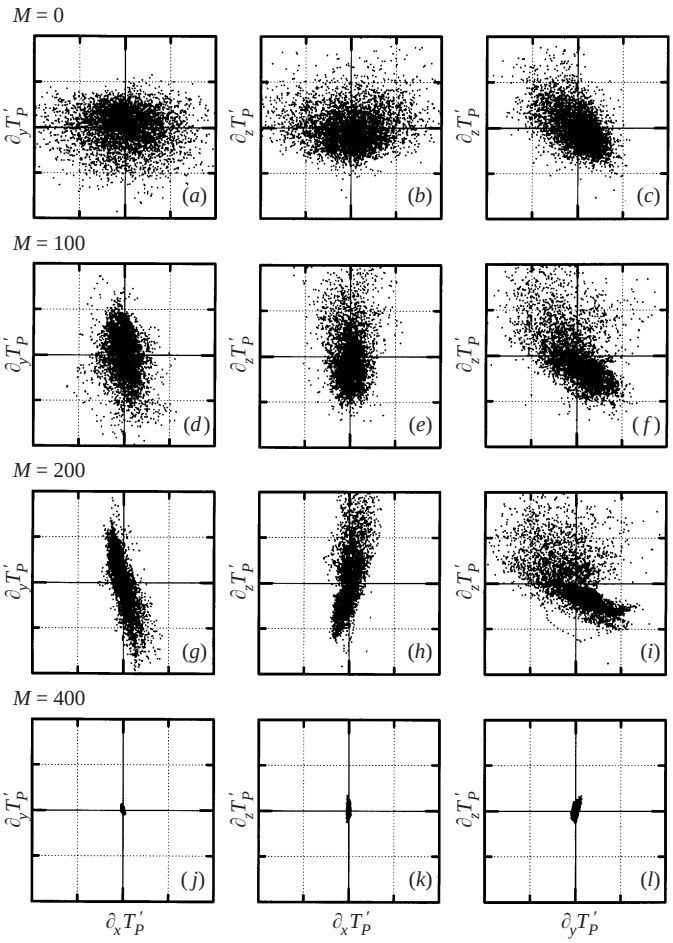

FIGURE 11. Scatter plots of the two-dimensional temperature gradient vectors $\nabla_{ij} T'_P = (\partial_i T'_P, \partial_j T'_P)$, namely $\nabla_{xy} T'_P$ (first column), $\nabla_{xz} T'_P$ (second column) and $\nabla_{yz} T'_P$ (third column). The first row corresponds to $M = 0$ (*a–c*), the second to $M = 100$ (*d–f*), the third to $M = 200$ (*g–i*) and the fourth to $M = 400$ (*j–l*). All figures show the same range in both directions, $-1.0 < \partial_i T'_P < 1.0$.

figure 7(*c*). For $M = 400$ (figure 11*j–l*) the flow is quasi-stationary as can be seen also from figure 9(*d*).

The discussion of local isotropy using the isotropy coefficients A_{ij} defined by equation (7) for regarding figure 7(*a–c*) can be extended into the frequency range. Here we introduce the frequency-dependent spectral isotropy coefficient functions

$$A_{ij}(f) = \frac{S_i(f)}{S_j(f)}, \tag{8}$$

where $S_i(f)$ are the components of the power spectra of the i-component of the spatial derivative of the temperature field. In figures 12(*a*) and 12(*b*) the two transversal spectral isotropy coefficient functions A_{xy} and A_{xz} are plotted for OHD flow ($M = 0$) and MHD flows at $M = 50$ and $M = 100$. Figure 12(*c*) shows the corresponding vertical coefficient functions. In conformity with figures 7(*a*) and 7(*b*) and the corresponding diagrams in figure 11 the transversal isotropy coefficients are considerably decreased by the magnetic field and thus indicate significant local non-isotropy. All measure-

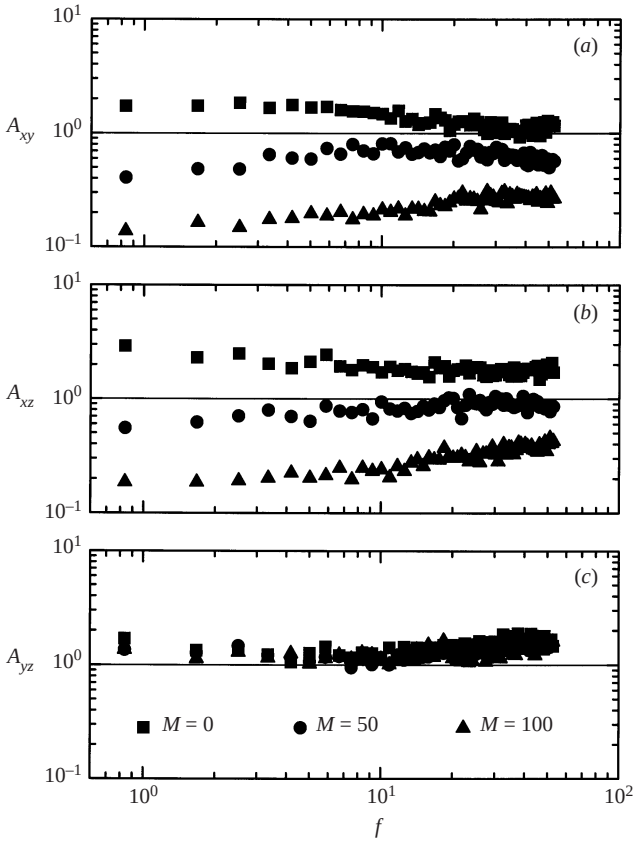

FIGURE 12. Spectral isotropy coefficient functions $A_{ij}(f)$ defined by equation (8) for OHD flow ($M = 0$) and MHD flows at $M = 100$ and $M = 200$: (a, b) transversal coefficients A_{xy} and A_{xz}; (c) vertical coefficient A_{yz}.

ments show higher isotropy at either higher frequencies or smaller length scales. This is consistent with recent results obtained by Burr *et al.* (2000) in turbulent MHD duct flow. Consistent with the findings in figure 7(c) the vertical isotropy property is hardly affected by the magnetic field. The coefficients depend weakly on frequency in the region $4 \lesssim f \lesssim 15$ where fluctuations of high vertical isotropy, i.e. $A_{yz} \approx 1$, are observed.

Further information on the temporal structure of the flow is obtained from the probability density functions (PDFs) of the probe signals. In figure 13(a–c) the PDFs of the temperature fluctuations T'_P from the measurement series at $Ra = 4.0 \times 10^4$ are plotted for OHD flow ($M = 0$) and the two Hartmann numbers $M = 100$ and $M = 200$. The circles represent measured values whereas the solid lines are Gaussian fitting curves. Under OHD conditions (figure 13a) the measured PDF of the temperature fluctuations is represented well by the Gaussian fitting curve. As a magnetic field is applied the PDFs in figures 13(b) and 13(c) become much broader and skewed, compared to those without magnetic field. This indicates more fluctuations of higher amplitude in the case of MHD flow compared to OHD flow. Moreover, the distributions of MHD flow deviate more strongly from a Gaussian distribution. In table 3 the values of skewness $S(T_P) = \overline{T_P'^3}/\overline{T_P'^2}^{3/2}$ and flatness $F(T_P) = \overline{T_P'^4}/\overline{T_P'^2}^2$ of the temperature fluctuations are compiled. A Gaussian PDF is indicated by $S = 0$

	T'_P		$\partial_x T'_P$		$\partial_y T'_P$		$\partial_z T'_P$	
M	S	F	S	F	S	F	S	F
0	0.11	2.53	0.04	3.52	−0.58	3.33	0.80	4.17
100	−0.01	2.43	0.18	4.80	−0.58	3.52	1.27	4.95
200	−0.20	2.28	0.72	4.10	−0.50	3.24	0.88	3.50

TABLE 3. Skewness and flatness of the fluctuating parts of the temperature and temperature gradient signals, T'_P and $\partial_i T'_P$ respectively of the probe for a Rayleigh number $Ra = 4.0 \times 10^4$ and different Hartmann numbers M.

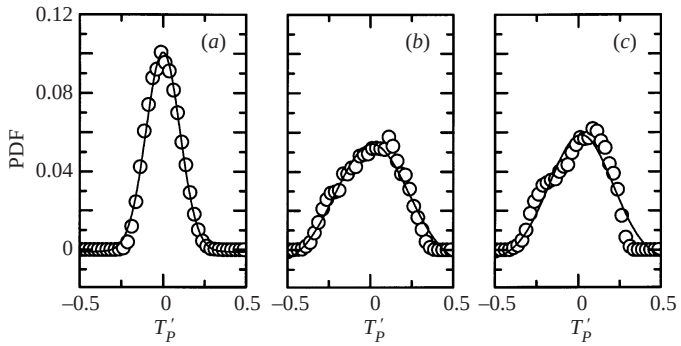

FIGURE 13. Probability density functions (PDFs) of the temperature fluctuations T'_P of the probe. At $Ra = 4.0 \times 10^4$ the Hartmann number is increased from (*a*) OHD flow at $M = 0$ to MHD flows with (*b*) $M = 100$ and (*c*) $M = 200$. The circles are the measured PDFs and the solid lines are their Gaussian fitting curves.

and $F = 3$ whereas $S \neq 0$ indicates a skewed distribution of fluctuations around the mean and $F < 3$ or $F > 3$ indicate a flatter or peakier distribution than Gaussian. The change in sign of S shows that the positively skewed distribution of T'_P for $M = 0$ changes to negative under the influence of the magnetic field. Indicated by $F < 3$, the PDFs of both OHD and MHD flow are flatter than for a Gaussian distribution.

Similar considerations can be made for the level of temperature gradients recorded by the probe. In figure 14(*a–c*) the PDFs of the fluctuating part of the temperature gradient in the transversal direction $\partial_x T'_P$ are plotted. Figures 14(*d–f*) and 14(*g–i*) show the same property in the horizontal y-direction $\partial_y T'_P$ and the vertical z-direction $\partial_z T'_P$. The corresponding values of skewness and flatness are also compiled in table 3. In the direction parallel to the magnetic field the PDF degenerates from its near-Gaussian shape for OHD flow to a peak-like shape indicating less strong deviations from the mean value. In the two directions perpendicular to the magnetic field large fluctuations persist even at high magnetic fields and the PDFs remain broad. Compared to the PDFs in the direction of the magnetic field, this again indicates strong local non-isotropy.

In both directions y and z, the distributions of the temperature gradients are much more skewed than the fluctuations of the temperature field itself. This is seen especially in the PDFs in the z-direction and the corresponding large values of skewness factors in table 3. As indicated by the flatness factors $F > 3$ fluctuations of the temperature gradients in all directions are peakier than a Gaussian distribution, in contrast to those of the temperature field which are determined to be flatter than a Gaussian distribution. However, at the level of temperature gradients and for the parameters

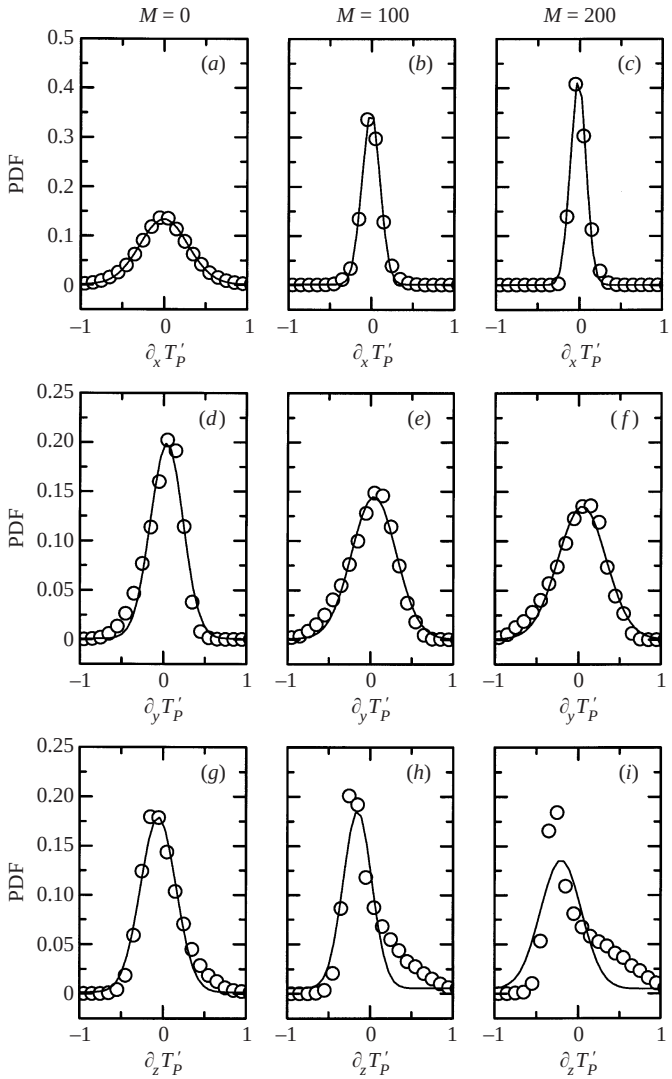

FIGURE 14. PDFs of the fluctuating parts of the temperature gradients recorded by the probe at $Ra = 4.0 \times 10^4$: (*a–c*) gradient in the transversal direction $\partial_x T'_P$, parallel to the magnetic field; (*d–f*) and (*g–i*) gradients in the directions perpendicular to the magnetic field $\partial_y T'_P$ and $\partial_z T'_P$. The magnetic field is increased from OHD flow at $M = 0$ (a, d, g) to $M = 100$ (b, e, h) and $M = 200$ (c, f, i) from left to right. The circles are the measured PDFs whereas the solid lines are their Gaussian fitting curves.

investigated here a clear tendency of the magnetic field to produce non-Gaussian PDFs, as observed for the temperature field, is only obtained in the z-direction.

4. Concluding remarks

Natural convection of an electrically well-conducting fluid in a tall vertical enclosure is significantly influenced by a uniform horizontal magnetic field applied perpendicularly to the horizontal temperature gradient. For the investigated range of Rayleigh numbers $10^3 < Ra < 8.0 \times 10^4$ the convective heat transport is significantly enhanced

for Hartmann numbers $M \lesssim 400$, even compared to ordinary hydrodynamic (OHD) flow. From estimates of the local isotropy properties of the flow using a four-element temperature probe it can be demonstrated that strong local anisotropy is produced by the magnetic field, consistent with the well-known tendency of vorticity lines to align with the direction of the magnetic field. The reduced three-dimensional nonlinearities of the locally non-isotropic flow favour the formation of larger-scale vortex structures compared to OHD flow, which are more effective in convective heat transport. This is demonstrated by a power shift from shorter to longer time scales in the power spectra of temperature fluctuations when the magnetic field is imposed. Thus, the damping effect of Joule dissipation on the convective motions is counterbalanced by an ordering effect of the magnetic field which may dominate and improve heat transfer rates.

At moderate Hartmann numbers the fluctuating intensities of MHD flows exceed those of OHD flow but for Hartmann numbers beyond $M \approx 400$ the flow becomes stationary. Above this Hartmann number there is still significant convective heat transport in stationary flow. Further increase of the Hartmann numbers leads to suppression of the convective heat transfer and a state close to pure heat conduction is approached.

Under OHD conditions a significant contribution from large-scale convection covering the total slot height to the heat transport is indicated by the formation of a vertical temperature gradient in the gap. Under the influence of a not too small magnetic field this contribution is reduced, indicating that smaller structures become more important for convective heat transport. As the flow proceeds from time-dependent to stationary conditions the vertical stratification is increased, again suggesting a breakdown of the multicellular flow pattern and formation of a unicellular motion.

The magnetic field causes the probability density function (PDF) of temperature fluctuations to increasingly deviate from a distribution close to a Gaussian in the absence of magnetic field. The deviations from the Gaussian behaviour are much stronger for the fluctuations of temperature derivatives.

The results clearly show that the application of a horizontal magnetic field to convective flows can be very helpful in the improvement of material processes. For instance, a heat transfer enhancement may speed up the process or the generation of stationary conditions with significant convective velocities will allow good mixing of low-diffusive species under stationary conditions commonly not obtained in liquid metal flows.

The authors are grateful to Professor U. Müller for initiating this research and for valuable discussions and comments and to Mr K. J. Mack for excellent technical support. This article is based on the master thesis of Dipl.-Ing. Paul Jochmann performed at the Institut für Kern- und Energietechnik of the Forschungszentrum Karlsruhe.

REFERENCES

Bergholz, R. F. 1977 Instability of steady natural convection in a vertical fluid layer. *J. Fluid Mech.* **84**, 743–768.

Burr, U., Barleon, L., Müller, U. & Tsinober, A. 2000 Turbulent transport of momentum and heat in magnetohydrodynamic rectangular duct flow with strong sidewall jets. *J. Fluid Mech.* **406**, 247–279.

Burr, U. & Müller, U. 2001 Rayleigh–Bénard-convection in liquid metal layers under the influence of a vertical magnetic field. *Phys. Fluids* **13**, 3247–3257.

Burr, U. & Müller, U. 2002 Rayleigh–Bénard-convection in liquid metal layers under the influence of a horizontal magnetic field. *J. Fluid Mech.* **453**, 345–369.

Davidson, P. A. 1995 Magnetic damping of jets and vortices. *J. Fluid Mech.* **299**, 153–186.

Elder, J. W. 1965 Laminar free convection in a vertical slot. *J. Fluid Mech.* **23**, 77–98.

Emery, A. F. 1963 The effect of a magnetic field upon the free convection of a conducting fluid. *J. Heat Transfer*, pp. 565–576.

Foust, O. 1972 *Sodium-NaK Engineering Handbook*, Vol. 1. Gordon and Breach.

Fumizawa, M. 1980 Natural convection experiment with liquid NaK under transverse magnetic field. *J. Nuclear Sci. Technol.* **17**, 98–105.

Gebhart, B., Jaluria, Y., Mahajan, R. & Sammakia, B. 1988 *Buoyancy-induced Flows and Trans-Port*. Hemisphere.

Gill, A. E. 1974 A theory of thermal oscillations in liquid metals. *J. Fluid Mech.* **64**, 577–588.

Horanyi, S., Krebs, L. & Müller, U. 1999 Turbulent Rayleigh–Bénard convection in low Prandtl-number fluids. *Intl J. Heat Mass Transfer* **42**, 3983–4003.

Hurle, D. T. J., Jackeman, E. & Johnson, C. P. 1974 Convective temperature oscillations in molten gallium. *J. Fluid Mech.* **64**, 565–576.

Kishida, Y. & Takeda, K. 1994 Suppression of turbulent Bénard convection by horizontal DC magnetic field. *Proc. Intl Symp. on Electromagnetic Processing of Materials, October 25–28, Nagoya, Japan, ISIJ* (ed. S. Asai), pp. 80–85. The Iron and Steel Institute of Japan.

Lyon, N. 1952 *Liquid Metals Handbook*, 2nd edn. Navexos P-733.

O'Donnel, J. O., Papanicolaou, P. G. & Reed, C. B. 1989 The thermophysical and transport properties of eutectic NaK near room temperature. *Tech. Rep.* ANL/FPP/TM-237.

Okada, K. & Ozoe, H. 1992 Experimental heat transfer rates of natural convection of molten gallium suppressed under an external magnetic field in either the x, y, or z direction. *J. Heat Transfer* **114**, 107–114.

Ozoe, H. & Okada, K. 1989 The effect of direction of the external magnetic field on the three-dimensional natural convection in a cubical enclosure. *Intl J. Heat Mass Transfer* **32**, 1939–1954.

Papailiou, D. D. & Lykoudis, P. S. 1968 Magneto-fluid-mechanic laminar natural convection – an experiment. *Intl J. Heat Mass Transfer* **11**, 1385–1391.

Papailiou, D. D. & Lykoudis, P. S. 1974 Turbulent free convection flow. *Intl J. Heat Mass Transfer* **17**, 161–172.

Sommeria, J. & Moreau, R. 1982 Why, how and when, MHD turbulence becomes two-dimensional. *J. Fluid Mech.* **118**, 507–518.

Vest, C. & Arpaci, V. S. 1969 Stability of natural convection in a vertical slot. *J. Fluid Mech.* **36**, 1–15.

Walker, J. S. 1981 Magnetohydrodynamic duct flows in rectangular ducts with thin conducting walls I. *J. Méc.* **20**, 79–112.